RSC Advances

PAPER

View Article Online
View Journal | View Issue



Cite this: *RSC Adv.*, 2024, **14**, 29636

# Harnessing the synergistic potential of $TiO_2$–CuSe composites for enhanced photocatalytic and antibacterial activities

Asma Kiran,[a] Ayesha Riaz,[b] Zahid Ali,[c] Rabia Maryam,[d] Furqan Ahmad,[e] Rafaqat Hussain,*[a] Nasir Ali Siddiqui,[f] Afzal Hussain,[f] Sonia Zulfiqar[ghi] and Eric W. Cochran*[h]

With growing environmental concerns, the removal of toxic industrial dyes from wastewater has become a critical global issue. In this study, $TiO_2$–CuSe composites were synthesized using a cost-effective and simple chemical method to determine the optimal concentration of CuSe for the efficient degradation of methylene blue (MB) under visible light. The $TiO_2$ samples exhibited a mix of rutile and anatase phases, while CuSe formed in a hexagonal phase. Both $TiO_2$ and CuSe were observed to have agglomerated particles with indistinct boundaries. The optical bandgap shifted towards the visible region from 3.25 eV (pure $TiO_2$) to 2.91 eV with increasing the amount of CuSe in the composites. The photocatalytic activity of $TiO_2$, CuSe, and $TiO_2$–CuSe composites was evaluated by monitoring MB degradation, with the composites outperforming the individual components under visible light. Notably, the $TiO_2$–20% CuSe composite (AK-4) demonstrated superior efficiency, removing 98% of MB in just 70 minutes. The photocatalysts also exhibited enhanced antibacterial properties, effectively reducing *E. coli* colonies from $1.71 \times 10^{12}$ CFU $mL^{-1}$ (pure $TiO_2$) to $1 \times 10^{10}$ CFU $mL^{-1}$ for the AK-4 composite. This study suggests that visible light-activated $TiO_2$–CuSe composites could be effective for both water purification and bacterial infection control.

Received 17th July 2024
Accepted 9th September 2024

DOI: 10.1039/d4ra05194g

rsc.li/rsc-advances



## 1. Introduction

Water pollution is regarded as an important environmental issue created by numerous industries.[1] According to recent surveys, approximately 300 000 tons of dyes are directly released into freshwater resources without proper treatment.[2] The discharge of these industrial effluents into freshwater resources is known to exhibit harmful effects on the environment, posing a major health risk to humans and threatening the existence of numerous aquatic species.[3] Furthermore, their high capability for sunlight absorption affects photosynthesis in water, which limits the production of oxygen. It has been reported that more than two billion humans are unable to access pure drinking water.[4] In view of all these factors, there is a need for the development of low-cost and effective water purification techniques.[5] A number of techniques for wastewater treatment have been developed to date, but they are mainly limited due to their high cost and production of additional waste. To overcome these issues, photocatalysis is a prominent choice due to its high efficiency, low cost, working under solar light, simplicity, *etc.*[6,7] For developing effective photocatalysts, metal oxides are highly attractive nominees as they exhibit interesting physiochemical properties and desirable photocatalytic performances. However, their wide bandgap nature and rapid recombination of charge carriers are known to impede their photocatalytic performance.[8] In order to address these challenges, various functional materials have been explored and engineered to enhance their photocatalytic activity in visible light.

Titanium dioxide ($TiO_2$) is a commonly used semiconductor material because of its excellent electronic and optical properties, high photo reactivity, excellent chemical stability, high refractive index, low cost, and non-toxicity.[9] It has been found to be an effective candidate for wastewater treatment, however, due to its inherent features, such as low quantum efficiency and

[a]*Department of Chemistry, COMSATS University Islamabad, Park Road, Islamabad 45550, Pakistan. E-mail: rafaqathussain@comsats.edu.pk*
[b]*Department of Physics, Faculty of Engineering and Applied Sciences, Riphah International University, I-14 Campus, Islamabad, Pakistan*
[c]*Department of Biosciences, COMSATS University Islamabad, Park Road, Islamabad 45550, Pakistan*
[d]*Department of Physics, University of Milano Bicocca, Piazza della Scienza 3, Milano I-20126, Italy*
[e]*Department of Physics, COMSATS University Islamabad, Park Road, Islamabad 45550, Pakistan*
[f]*Department of Pharmacognosy, College of Pharmacy, King Saud University, PO Box 2457, Riyadh 11451, Saudi Arabia*
[g]*Department of Physical Sciences, Lander University, 320 Stanley Ave, Greenwood, South Carolina 29649, USA*
[h]*Department of Chemical and Biological Engineering, Iowa State University, Sweeney Hall, 618 Bissell Road, Ames, Iowa 50011, USA. E-mail: ecochran@iastate.edu*
[i]*Department of Chemistry, Faculty of Science, University of Ostrava, 30. Dubna 22, Ostrava, 701 03, Czech Republic*

large band gap (3.2 eV), the photocatalytic activity of $TiO_2$ is limited to UV light, which is not sufficient for its effective utilization in wastewater remediation.[10,11] To shift the bandgap (3.2 eV) from the UV to the visible range for better photocatalytic properties, strategies such as deposition of noble metals, combining $TiO_2$ with other semiconductors, and doping with metals or nonmetals *etc.* have been often performed.[9,12] Shifting of the bandgap to the visible part of the spectrum enables the material to absorb visible light and produce photogenerated carriers for redox reactions.[13] $TiO_2$-based heterogeneous systems are of special interest due to their exceptional photocatalytic activity since they offer the advantage of overcoming the easy recombination of $e^-/h^+$ pairs and provide additional active sites for enhanced reaction processes.[14]

In recent times, transition metal chalcogenides have spurred ongoing scientific interest due to their promising physiochemical features and high potential in a range of technological applications.[15] Copper selenide (CuSe) is an important p-type semiconductor having both direct (1.7–3.0 eV) and indirect (1.1–1.5 eV) bandgap.[16] The bandgap energy and thermal stability of CuSe have been reported to change with their structural phases or stoichiometries.[17] It exists in several stoichiometric (CuSe, $CuSe_2$ and $Cu_3Se_2$) and non-stoichiometric compositions ($Cu_{2-x}$ Se) and thus can be arranged into a variety of crystallographic modifications such as cubic, tetragonal, hexagonal, and orthorhombic.[18] CuSe is hexagonal at room temperature, transitioning to orthorhombic at 48 °C, and then back to hexagonal at 120 °C.[19] Though CuSe is an attractive material with exceptional characteristics, it has rarely been utilized as a photocatalyst for wastewater remediation.[20]

Coupling $TiO_2$ with other functional materials to produce novel heterostructures is considered a viable alternative for enhanced degradation efficiencies. These photocatalysts are advantageous due to several factors, including their lower bandgap energies, large specific surface area, and their capability to effectively facilitate the interfacial charge transfer, thus suppressing the recombination of photoinduced charge carriers. Although significant efforts and strategies are directed toward enhancing the photocatalytic efficiency of $TiO_2$ under visible light exposure, its coupling with CuSe at different concentrations remains an unexplored frontier. In view of the abovementioned traits, pure $TiO_2$, CuSe, and their composites were prepared *via* simple and low-cost chemical methods. We have explored the synergistic relationship of $TiO_2$–CuSe heterostructures for superior photocatalytic and antibacterial characteristics. The findings suggest that compared to $TiO_2$ and CuSe, the absorption properties of $TiO_2$–CuSe composite samples are considerably shifted towards the visible region with increasing CuSe content. The photocatalytic and antibacterial characteristics of the $TiO_2$–CuSe composites are significantly enhanced compared to $TiO_2$ and CuSe, respectively.

## 2. Experimental section

### 2.1. Materials

Cupric chloride dihydrate ($CuCl_2 \cdot 2H_2O$, Samchun), sodium hydroxide (NaOH, AppliChem), selenium powder (Se, Sigma-

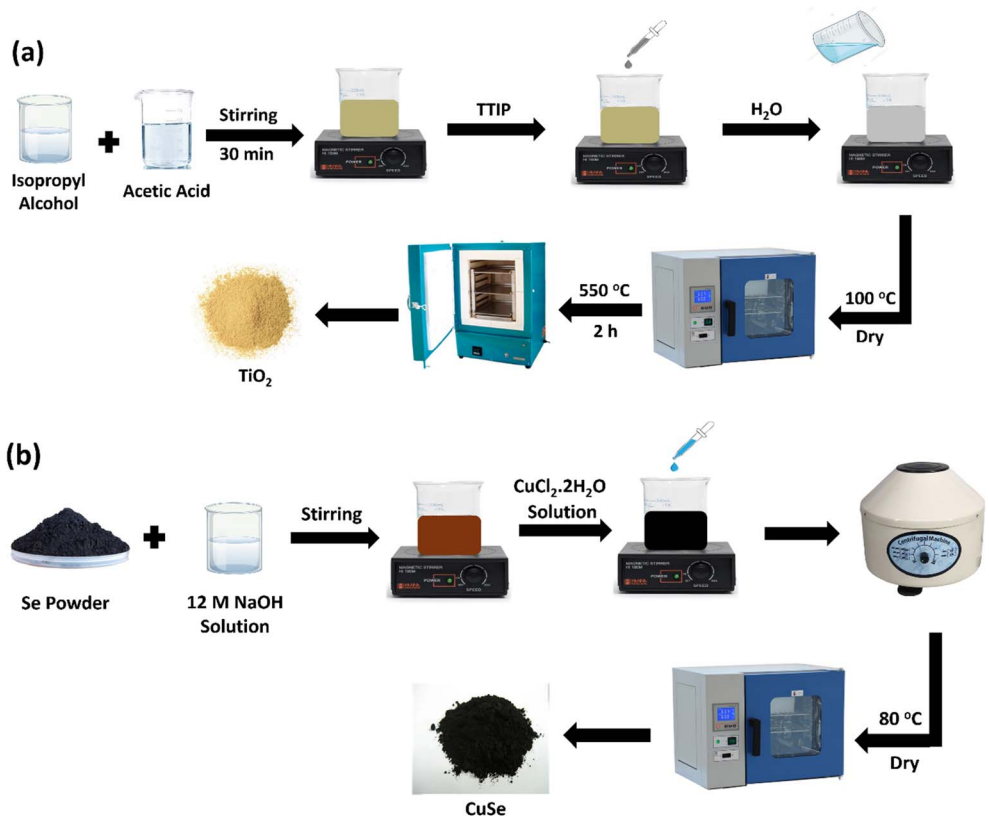


Fig. 1 Schematic illustration for the preparation of (a) $TiO_2$ NPs (b) CuSe NPs.

Aldrich), isopropyl alcohol (IPA, Medipak Limited), titanium tetraisopropoxide (TTIP, $C_{12}H_{28}O_4Ti$, Sigma-Aldrich), acetic acid ($CH_3COOH$, Duskan), methylene blue (Unichem) were of analytical grade and were used as received.

### 2.2. Synthesis of $TiO_2$

A simple sol–gel method was used to prepare $TiO_2$ nanoparticles (NPs), as shown in the schematic illustration (Fig. 1a). In a typical synthesis, a mixture of isopropyl alcohol (50 mL) and acetic acid (15 mL) was stirred for 30 min. TTIP (12.5 mL) was then added to the mixture in a dropwise manner under continuous stirring for further 30 min. After that, DI water (10 mL) was added dropwise to the above mixture. A white gel was obtained after 5 min of vigorous stirring, which was dried for 24 h in an oven at 100 °C. The final product was calcined at 550 °C for 2 h to obtain the crystalline $TiO_2$ powder.

### 2.3. Preparation of CuSe

For the synthesis of CuSe NPs, an easy chemical precipitation method was used (Fig. 1b).[21] First, an orange-colored aqueous alkaline Se solution was prepared by adding Se powder (3.948 g) to 12 M NaOH (50 mL). In another beaker, 8.5 g $CuCl_2 \cdot 2H_2O$ was first homogenously mixed in 50 mL DI water and then it was dropwise added to the alkaline Se solution under continuous stirring for 20 min. The formed black precipitates were centrifuged, washed with DI water followed by ethanol, and then dried at 80 °C for 24 h.

### 2.4. Preparation of $TiO_2$–CuSe composites

A number of $TiO_2$–CuSe composites with different concentrations of CuSe were synthesized. For this, certain amount of the prepared CuSe and $TiO_2$ powders were mixed in 40 mL of methanol, sonicated for 30 min, and then stirred for 30 min. The mixture was then dried overnight at 60 °C to furnish the composite. $TiO_2$–CuSe composites containing 5, 10, 15, and 20% CuSe were denoted as AK-1, AK-2, AK-3, and AK-4, respectively.

### 2.5. Characterization

The crystalline structure and phase information of CuSe, $TiO_2$, and their composites were analyzed by X-ray diffraction (XRD Phillips made) with $CuK_\alpha$ as a radiation source having $\lambda = 1.54$ Å. The XRD patterns were recorded over $2\theta$ values ranging from 20° to 80° with a step size of 0.03° $s^{-1}$. The vibrational properties were investigated with the help of Raman spectroscopy (Dongwoo Optron Co. Ltd) at room temperature. The instrument houses an argon-ion laser as a source having $\lambda = 514$ nm. The spectra were recorded over a range of 100–2000 $cm^{-1}$. Energy Dispersive X-ray Spectrometry (EDX) was used to study the elemental compositions of samples. For the evaluation of the morphological features, TESCAN-designed field-emission scanning electron microscopy (Model: MAIA3) was used. The images were obtained at an accelerating voltage of 20 kV at different magnifications for a better understanding of the sample morphology. The optical response of the samples was measured with the help of a Shimadzu UV-1280 UV spectrophotometer. The measurements were made over a wavelength range between 250 and 600 nm with a step size of 1 nm.

### 2.6. Evaluation of the photocatalytic activity

The visible light-mediated photocatalytic performance of the prepared samples was examined by monitoring the degradation of MB dye. For this purpose, the experimental parameters were kept unchanged, allowing for an equal assessment of each photocatalyst. Experiments were performed in a purpose-built wooden box, designed to prevent the outside light from entering the box. The box was equipped with a visible light source (85 W LED lamp) with a wavelength range between 410–800 nm and intensity of 48 W $cm^{-2}$. Additionally, the light was maintained at an appropriate level to prevent the MB dye solution from heating up. For the evaluation of photocatalytic performance, a stock solution of 100 ppm was prepared by dissolving MB (0.01 g) in DI water (100 mL). The photocatalyst (40 mg) and stock solution of MB dye (1 mL) were added to DI water (100 mL). To achieve the adsorption–desorption equilibrium, the resulting mixture was subsequently stirred for around 30 min in the dark.[22] Then, the initial absorption reading of the mixture was recorded prior to exposure to the visible light. This initial data was referred to as the zero-min reading. After that, the light source was turned on, and 2 mL was extracted and centrifuged to remove the photocatalyst every 20 min. The absorption spectrum of the extracted solution was recorded to calculate the concentration of MB dye. This procedure was continued until the MB solution lost its typical blue color, which indicated that the dye was completely degraded. The efficiency of $TiO_2$, CuSe and their composites was determined by using eqn (1):

$$\%\ \text{degradation} = \left(\frac{C_0 - C_t}{C_0}\right) \times 100 \quad (1)$$

where $C_0$ presents the initial concentration of MB before its exposure to visible light and $C_t$ present the concentration of MB after time $t$.

### 2.7. Antibacterial activity

The antibacterial activity of the CuSe–$TiO_2$ composites was performed against Gram-negative bacteria *E. coli* under visible light conditions. Using the quantitative viable count method, the antibacterial characteristics of samples were studied. The LB media was prepared in DI water and was subsequently sterilized in an autoclave along with Petri dishes. A two-fold dilution method was used to prepare a 5 mg $mL^{-1}$ concentration of NPs in dimethyl sulfoxide (DMSO). 100 μL of $10^9$ dilution of *E. coli* culture grown to optical density 0.7 was inoculated on the plate through the spread culture method. The NPs stock solution was inoculated on LB agar plates, incubated at 37 °C for 24 h and the number of colonies were recorded as colony-forming units (CFU) $mL^{-1}$ to determine the size of microbial population.

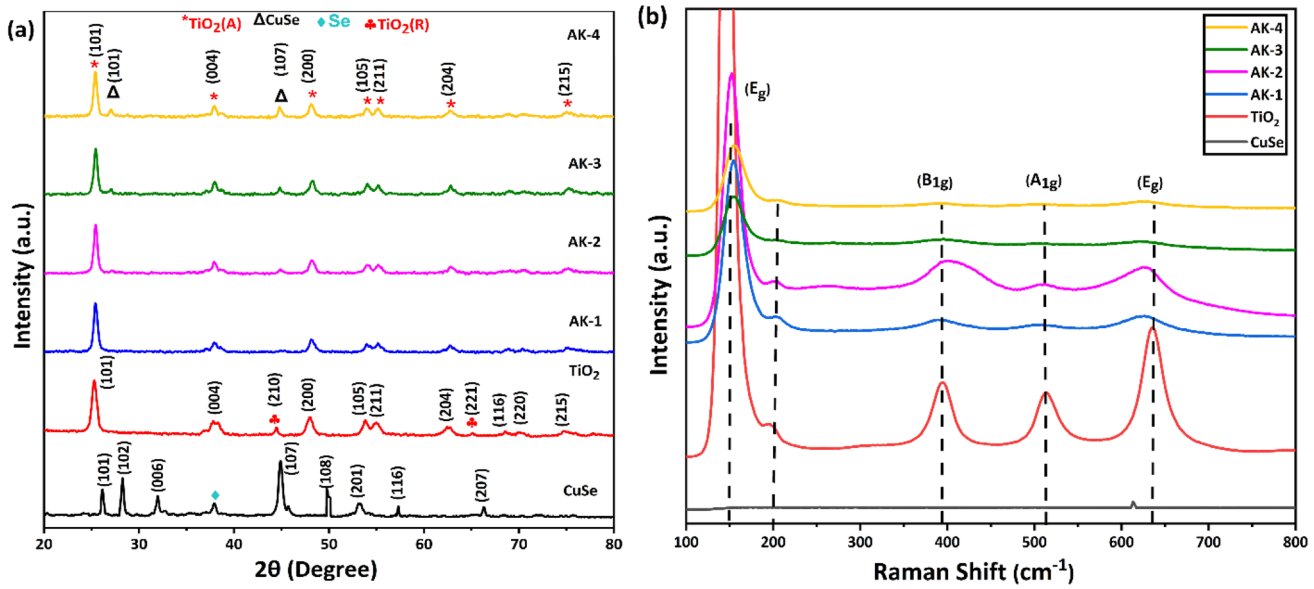


Fig. 2 (a) XRD patterns (b) Raman spectra of $TiO_2$, CuSe, and their composites.

## 3. Results and discussion

### 3.1. Structural, morphological and elemental analysis

The structural properties of the prepared materials were determined by recording XRD patterns between 20 and 80° (Fig. 2a). The XRD pattern of CuSe contains diffraction peaks at 26.17°, 28.18°, 31.18°, 44.99°, 49.98°, 53.00°, 57.23° and 66.24° which are respectively ascribed to the (101), (102), (006), (107), (108), (201), (116) and (207) planes of hexagonal structure of CuSe (JCPDS 34-0171). The peak present at 37.2° belongs to selenium.

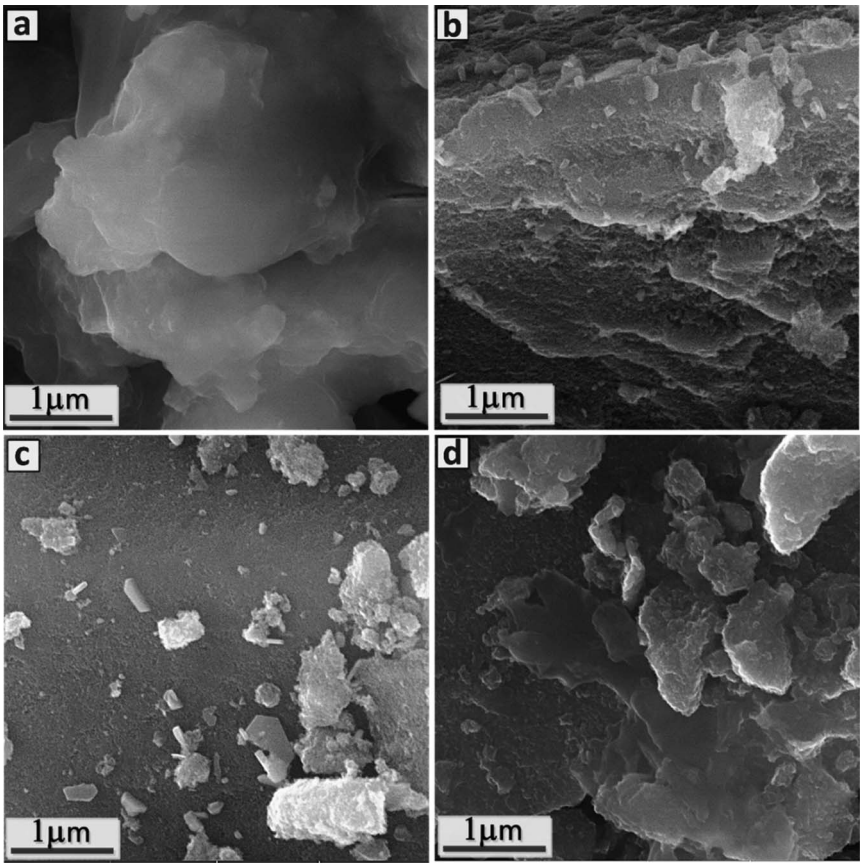


Fig. 3 FESEM images of (a) CuSe (b) $TiO_2$ (c) AK-1 (d) AK-4.

Furthermore, the lattice constants $a = b$ 3.9390 (Å) and $c$ = 17.2500 (Å) of CuSe also match well with the JCPDS 34-0171. The intense and broad diffraction peaks indicate the formation of nanocrystalline CuSe. Similarly, the XRD pattern of $TiO_2$ obtained by the sol–gel route revealed the formation of co-existing rutile and anatase phases of $TiO_2$. The diffraction peaks at $2\theta$ values of 25.23°, 37.86°, 48.06°, 53.97°, 54.96°, 62.36°, 68.62°, 70.20° and 74.78° are assigned to the (101), (004), (200), (105), (211), (204), (116), (220) and (215) lattice planes of the anatase phase of $TiO_2$ (JCPDS 01-071-1167). The diffractions observed at $2\theta$ values of 44.53°, 65.04° are respectively ascribed to the (210) and (221) planes of the rutile phase of $TiO_2$ (JCPDS 01-077-0443). The calculated lattice parameters ($a = b$ (Å) = 3.7760 and $c$ (Å) = 9.4860) of the anatase phase of $TiO_2$ are in good agreement with the standard. The most intense and well-defined peak corresponding to the (101) plane confirms the formation of crystalline $TiO_2$. The XRD patterns of CuSe–$TiO_2$ composites are shown in Fig. 2a, which contain well-defined peaks of $TiO_2$, whereas the diffractions due to the CuSe became more prominent as the content of CuSe increased. In addition, no noticeable change in the peak height, peak width, and location of the peaks was observed in the diffraction peaks of $TiO_2$, indicating that the incorporation of CuSe in the composite has no appreciable effect on the particle size and degree of crystallinity.

Fig. 2b shows the Raman spectra of the prepared samples. The spectrum of $TiO_2$ is comprised of four characteristic Raman active modes at 148, 398, 513, and 636 $cm^{-1}$, which are assigned $E_g$, $B_{1g}$, $A_{1g}$ and $E_g$ bands, respectively. The sharp and intense signal at 148 $cm^{-1}$ is assigned to the $E_g$ band, corresponding to the symmetric stretching vibration. Similarly, the vibrational band at 398 $cm^{-1}$ is mainly ascribed to $B_{1g}$ symmetric stretching mode. The signal centered at 513 $cm^{-1}$, is indicative of $A_{1g}$ antisymmetric bending vibration of O–Ti–O. Moreover, the high-frequency band at around 636 $cm^{-1}$ is assigned to symmetric stretching vibration ($E_g$). In the case of CuSe NPs, vibrational modes were not observed, as evident in Fig. 2b. Furthermore, the intensity of vibrational bands for $TiO_2$–CuSe composites was decreased with an increase in the content of CuSe.

FESEM images of $TiO_2$, CuSe, and $TiO_2$–CuSe composites were acquired to understand their morphological features. The corresponding results are presented in Fig. 3. It is observed that for both CuSe and $TiO_2$, the surface morphology comprised agglomerated particles, which could be attributed to the high surface energies of the NPs. For the $TiO_2$–CuSe composites, the morphology is similar to that observed for pure $TiO_2$ and CuSe. The formation of aggregates and agglomeration is ascribed to the high surface energy of NPs, chemical and van der Waals interactions. Due to the agglomeration phenomena, the size and shape of the NPs could be barely recognized in the FESEM images (Fig. 3).

In order to study the elemental composition, CuSe, $TiO_2$, and $TiO_2$–CuSe composites were subjected to the EDX analysis. The EDX spectrum of CuSe is shown in Fig. 4a, which contains peaks for Cu and Se elements. In the case of $TiO_2$, elemental peaks due to Ti and O were observed (Fig. 4b). The EDX spectra of $TiO_2$–CuSe composites are presented in Fig. 4c and d, where peaks due to Ti, O, Cu, and Se are evident. The intensity of peaks for Cu and Se increases as the concentration of the CuSe increases in the composite samples. Moreover, no peaks due to any other elements were observed, thus certifying the purity of the prepared samples.

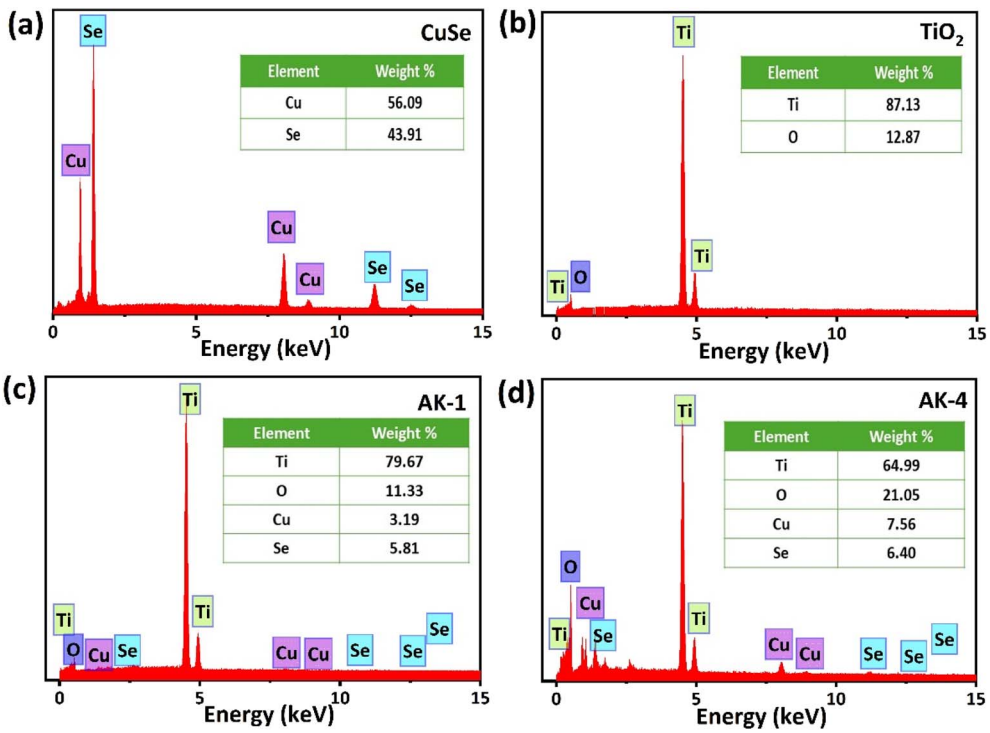


Fig. 4 EDX spectra of (a) CuSe (b) $TiO_2$ (c) AK-1 (d) AK-4.

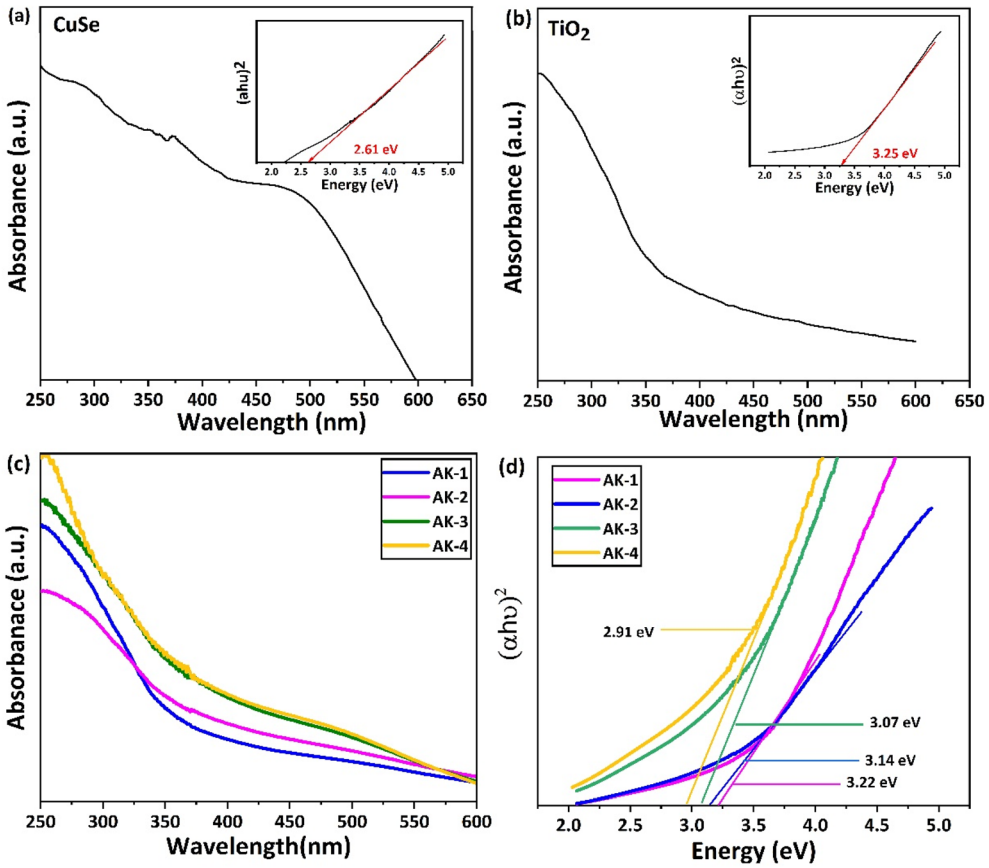


Fig. 5 (a) Absorption spectrum of CuSe. The inset shows the Tauc plot for determination of the bandgap of CuSe (b) absorption spectrum of $TiO_2$. The Tauc plot is presented in the inset (c) Absorption spectra of $TiO_2$–CuSe composites (d) Tauc plots of $TiO_2$–CuSe composites.

### 3.2. Optical analysis

Absorption spectra of CuSe, $TiO_2$ and their composites are shown in Fig. 5. The spectrum of CuSe shows the absorption edge in the visible range (Fig. 5a), indicating the low energy gap of CuSe. The bandgap energy ($E_g$) of CuSe was determined by using the following well-known Tauc eqn (2):

$$(\alpha h\nu)^2 = A(h\nu - E_g) \quad (2)$$

where, $h$ represents the Planck's constant, frequency of incident photons is represented by $\nu$, $\alpha$ corresponds to the absorption coefficient, $A$ is a constant and the superscript is associated with the nature of electronic transitions for a specific material. The value of $E_g$ for CuSe was determined to be 2.61 eV (inset of Fig. 5a). The spectrum of $TiO_2$ NPs is shown in Fig. 5b, where a strong light absorption is evident at around 350 nm. By using the Tauc plot (inset of Fig. 5b), the value of $E_g$ was calculated to be 3.25 eV. Compared to $TiO_2$ NPs, a shift towards the visible region is observed in the optical response for the $TiO_2$–CuSe composites (Fig. 5c). The lowest value of $E_g$ was determined for composite AK-4, which was found to be 2.91 eV for a high amount of CuSe.

### 3.3. Photodegradation studies

The photocatalytic response of MB in the presence of CuSe, $TiO_2$ and $TiO_2$–CuSe composites was systematically investigated, and the corresponding results are presented in Fig. 6 and 7. Prior to the addition of any photocatalyst, the absorption spectra of MB solution were first obtained after regular intervals to observe the influence of visible light on the photodegradation of MB (Fig. 6a). The typical absorption peak of MB was observed at 650 nm. The intensity of the absorption peak is slightly reduced after exposure for 140 min, which suggests the structural stability of MB is high and resistant to degradation. Likewise, Fig. 6(b) and (c) shows the response of CuSe and $TiO_2$ against MB. Following exposure to visible light for 140 min, the absorption intensity of MB was decreased compared to that without any photocatalysts. However, the presence of CuSe or $TiO_2$ in the solution was still not able to completely degrade the MB. This could be attributed to the large bandgap of $TiO_2$ and the fast recombination rate of photoexcited carriers in CuSe, which impedes their photocatalytic efficiencies.

Fig. 7 presents the photocatalytic response of $TiO_2$–CuSe composites. When the composite AK-1 was loaded, the removal of MB was highly stimulated. It is evident that the intensity of MB was gradually reduced with an increase in the exposure time, indicating the mineralization of the dye. Likewise, the activity of AK-2 against MB was significantly enhanced, and MB was almost degraded in around 100 min (Fig. 7b). The presence of AK-3 composite has also expedited the removal of MB, but the performance is comparable to that of AK-2 after 100 min of

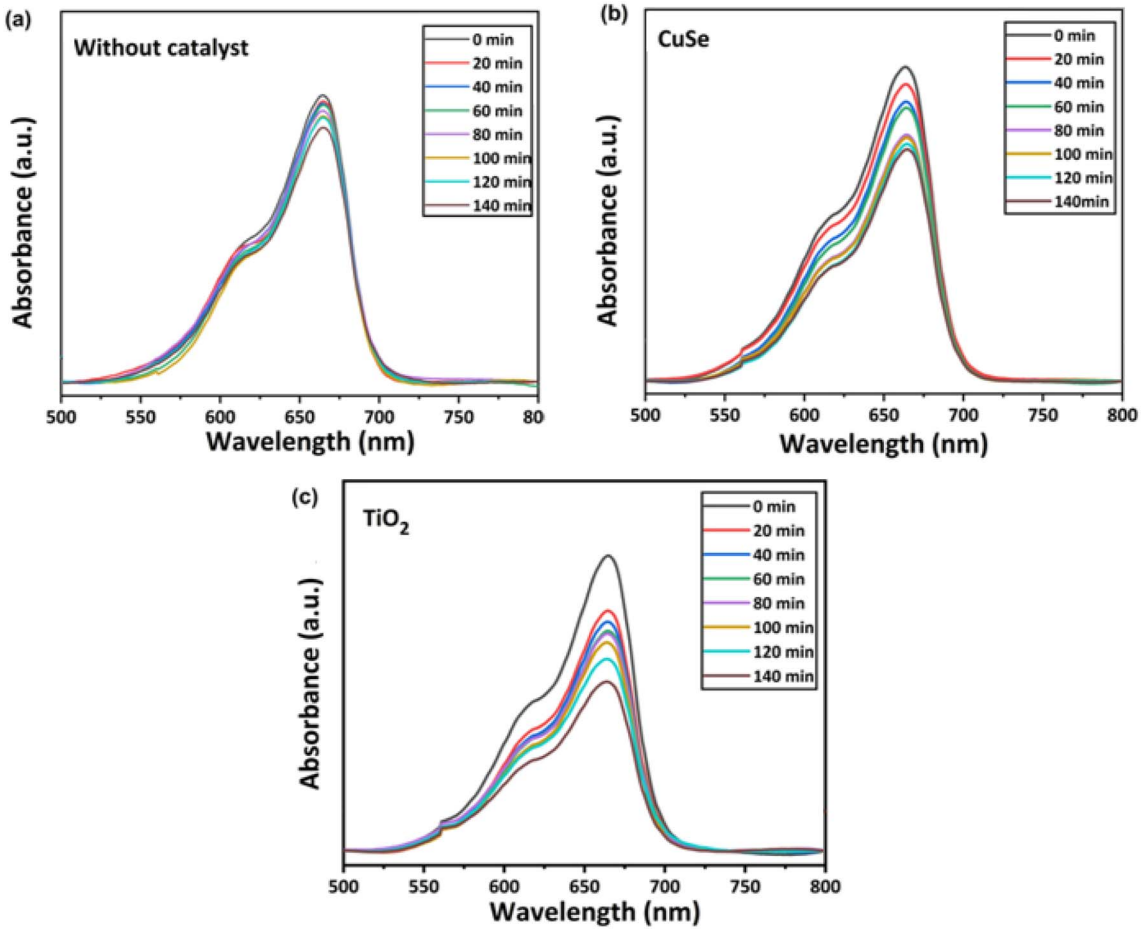


Fig. 6 Absorption spectra of MB solution obtained as a function of exposure time for (a) without any photocatalyst (b) using CuSe as a photocatalyst (c) $TiO_2$ as a photocatalyst.

exposure time (Fig. 7c). Among all the photocatalysts, the AK-4 composite revealed an impressive response, as shown in Fig. 7d. The absorption intensity of MB was substantially reduced in just 60 min of the exposure time.

Additional tests were performed to determine the relative concentrations of MB to examine the effectiveness of the prepared photocatalysts. The degradation rate ($C_t/C_o$) was plotted as a function of exposure time in Fig. 8a. For instance, the percentage degradation of MB without any photocatalyst was only 9% after light exposure of 140 min. Likewise, for CuSe and $TiO_2$ the degradation efficiency was determined to be 28 and 32%, respectively. For sample AK-1, 98% of MB is eliminated in 140 min, whilst the activity of AK-2 against MB was significantly enhanced and 96% of the dye was degraded in 100 min. Similarly, the removal efficiency was increased up to 98% in 100 min of exposure when AK-3 composite was used as a photocatalyst. Among all the photocatalysts, the AK-4 composite revealed superior performance, which removed 98% of MB in just 60 min of exposure time. The photocatalytic performance of all samples can be presented in the following order: AK-4 > AK-3 > AK-2 > AK-1 > $TiO_2$ > CuSe. By plotting $\ln(C_t/C_0)$ *versus* illumination time, the kinetic character of the prepared photocatalysts was investigated as shown in Fig. 8b. The degradation process followed the pseudo-first-order Langmuir–Hinshelwood model, which processes the reaction kinetics of heterogeneous reactions taking place at the surface of the catalyst. Additionally, the model can only be used if at least one of the reactants is present and its concentration remains constant, resulting in the conversion of the rate equation into a pseudo-first-order form. The reaction rate constant for every photocatalyst was calculated from Fig. 8b as shown in Table 1.

The scavenger study was also carried out to explore the intermediate reactive/oxidative species ($^{\bullet}OH$, $O_2^{\bullet-}$ and $h^+$) and elucidate the possible photocatalytic mechanism of $TiO_2$–CuSe photocatalyst. As shown in Fig. 8c, the degradation efficiency is reduced from 98% to 26% with the addition of ethylenediaminetetraacetic acid (EDTA), indicating that the $h^+$ played an active part in photodegradation. Similarly, the addition of isopropyl alcohol (IPA) also influenced the degradation efficiency, where a substantial reduction (45%) was observed. This suggests that the $^{\bullet}OH$ pathway is also crucial to the degradation process. Additionally, the degradation efficacy of the dye was marginally reduced when ascorbic acid (AA) was added to the MB solution, indicating that the role of superoxide radicals ($O_2^{\bullet-}$) is not significant in the photocatalytic process.

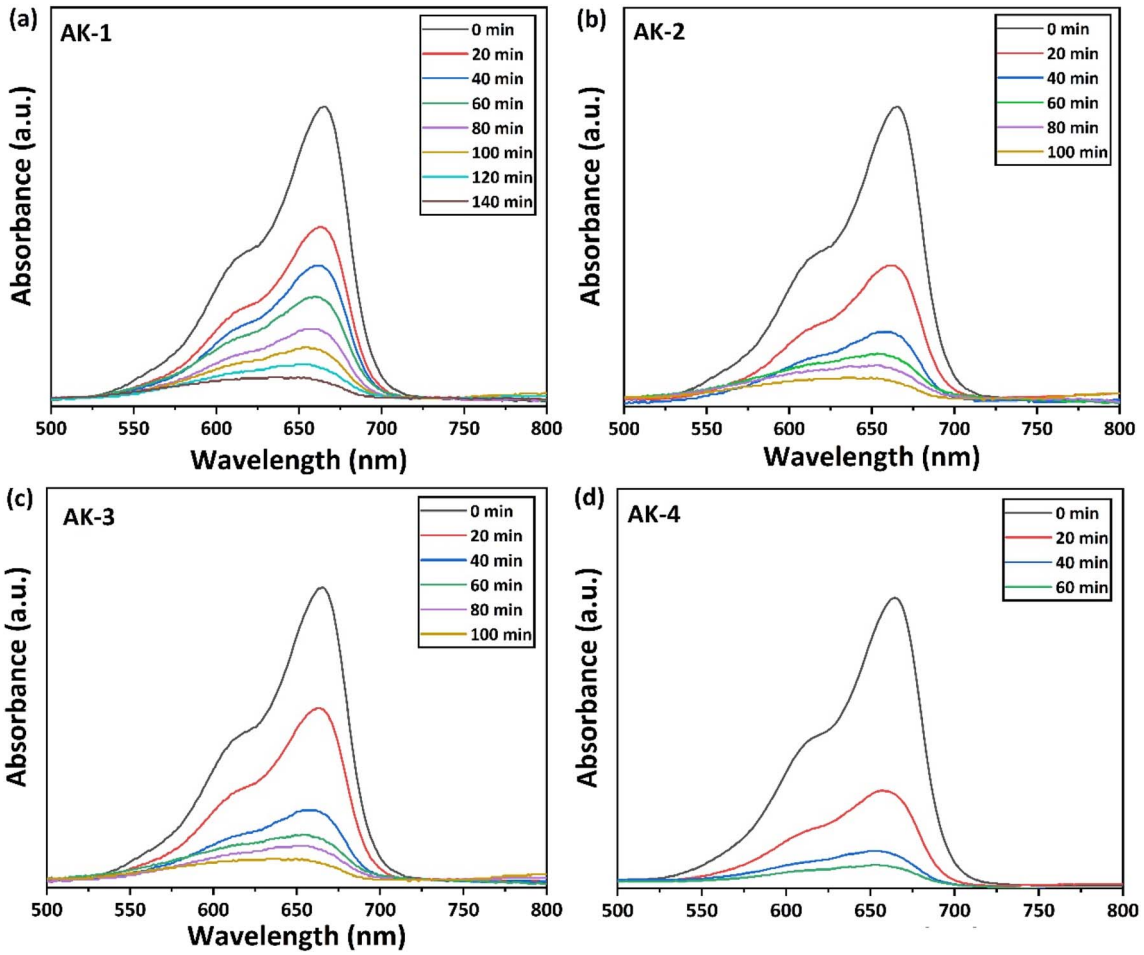


Fig. 7 Absorption spectra of MB as a function of time after loading of composites (a) AK-1 (b) AK-2 (c) AK-3 (d) AK-4.

Consequently, it could be concluded that reactive species, specifically $h^+$ and $^{\bullet}OH$, played strategically significant roles in the photodegradation of MB under visible light exposure.

Among all the photocatalysts, the AK-4 has a greater rate constant, which indicates its superior degradation efficiency. The high efficiency of AK-4 in degrading the MB indicates the presence of the large number of adsorption sites on the surface of the catalyst. This suggests that the presence of CuSe in the $TiO_2$–CuSe composites increases the numbers of $^{\bullet}OH$, which improves the photocatalytic activity. A comparison of the kinetic parameters is presented in Table 1.

Table 1 Kinetics data for the degradation of MB dye using the prepared photocatalysts

| Sample | $R^2$ | $k$ ($min^{-1}$) | Time (min) | Degradation (%) |
|---|---|---|---|---|
| Without catalyst | 0.97 | 0.000614 | 140 | 9 |
| CuSe | 0.96 | 0.00227 | 140 | 28 |
| $TiO_2$ | 0.91 | 0.00228 | 140 | 32 |
| AK-1 | 0.98 | 0.0208 | 140 | 98 |
| AK-2 | 0.95 | 0.0259 | 100 | 96 |
| AK-3 | 0.98 | 0.0288 | 100 | 98 |
| AK-4 | 0.95 | 0.0488 | 60 | 98 |

The above results suggest that compared to $TiO_2$ and CuSe, the $TiO_2$–CuSe composites are more efficient for the degradation of MB dye. The driving force responsible for such a remarkable performance is ascribed to the collective impact of two semiconductors with separate valence band (VB) and conduction band (CB) energy levels. On the other hand, the movement of charge carried between the two semiconductors was determined by using their corresponding edge potentials $E_{VB}$ and $E_{CB}$. Eqn (3) and (4) were used to calculate the $E_{VB}$ and $E_{CB}$.

$$E_{CB} = \chi - E^e - \frac{1}{2}E_g \quad (3)$$

$$E_{VB} = E_{CB} + E_g \quad (4)$$

The $E^e$ is the energy of the free electrons on the hydrogen scale, and its value is 4.5 eV. The absolute electronegativity values of $TiO_2$ and CuSe are 6.18 eV and 5.18 eV, respectively. The calculated values of $E_{CB}$ for $TiO_2$ and CuSe are 7.8 eV and 6.4 eV respectively. Likewise, the $E_{VB}$ values are 4.5 eV and 3.8 eV for $TiO_2$ and CuSe respectively.

It is evident from the visible light-mediated photocatalytic experiments that the degradation of MB dye requires the

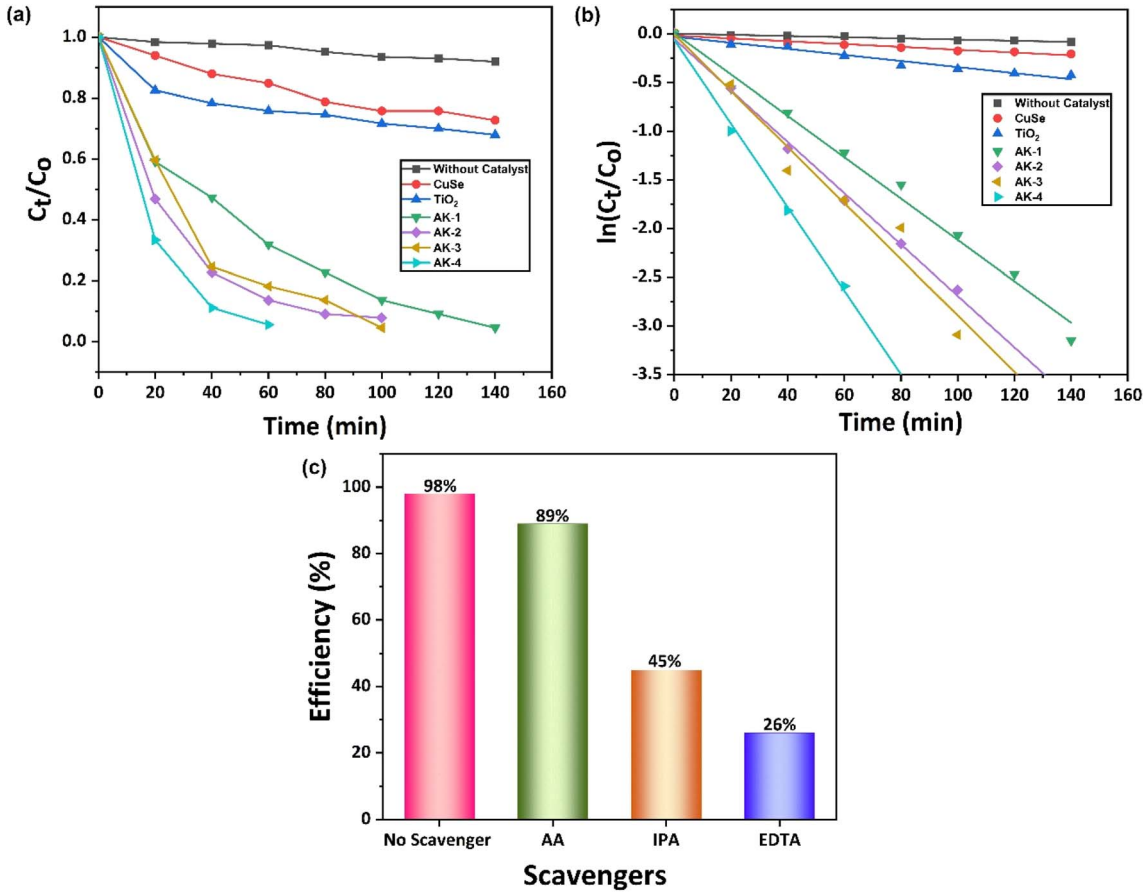


Fig. 8 (a) Photodegradation of MB as a function of time (b) $\ln(C_t/C_0)$ plotted against exposure time (c) scavenger analysis.

presence of a photocatalyst. The type (II) band alignment in $TiO_2$–CuSe heterojunction results in an effective spatial charge carrier separation (Fig. 9). The electrons excited by the visible light irradiation migrate from the CB of CuSe to the CB of $TiO_2$ during this process. The holes that build up in the $TiO_2$ VB can transfer to the CuSe VB due to the higher positive $E_{VB}$ value of $TiO_2$. The electron and accompanying hole separation between $TiO_2$ and CuSe is facilitated by the creation of the $TiO_2$–CuSe heterojunction interface. The realization of the charge separation enables the effective movement of the photoexcited electrons to the surface of the catalyst to initiate a series of redox reactions for the mineralization of MB. The electrons in the CB and holes in the VB, when exposed to visible light cause the degradation of MB. The ˙OH coupled with electrons and holes can systematically break the MB molecule through a series of redox reactions.[23] In Table 2, a comparison of the efficiency of AK-4 with previously reported work under visible light exposure is presented. It is apparent from the comparison that AK-4 exhibits superior efficiency as compared to previously reported work.

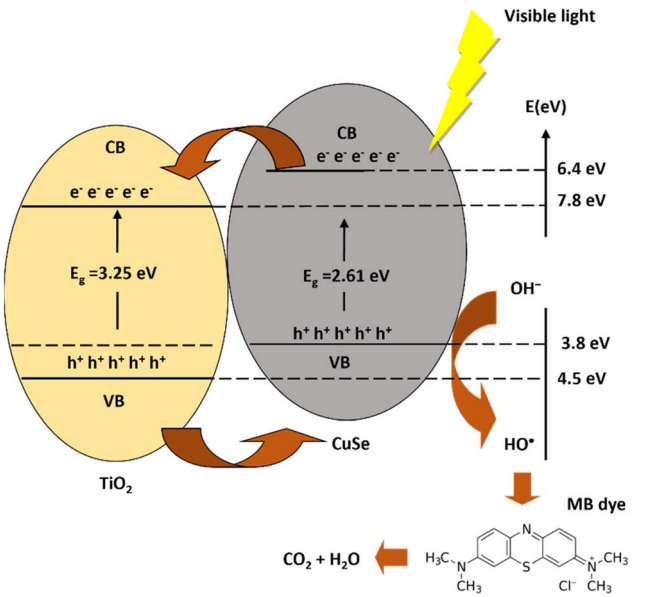


Fig. 9 Proposed mechanism for the degradation of MB dye by $TiO_2$–CuSe composites.

### 3.4. Antibacterial studies

Uncontrolled and incorrect dosages of conventional antibiotics over the years have resulted in the development of multidrug-resistant bacteria.[28] The treatment of multidrug-resistant bacteria or biofilm is a challenging task. However, the infection can be treated with the use of semiconducting NPs. The anti-bacterial activity of CuSe, $TiO_2$, and their composites was

Table 2 Comparison of the photocatalytic efficiency of AK-4 with other composite materials reported in the literature

| Sample | Degradation (%) | Time (min) | References |
|---|---|---|---|
| AK-4 | 98 | 60 | Present work |
| $BiVO_4/TiO_2$ | 84 | 120 | 24 |
| $TiO_2$/graphene | 96 | 150 | 25 |
| $TiO_2$–$Fe_2O_3$ | 88 | 300 | 26 |
| rGO-$Fe_3O_4/TiO_2$ | 98 | 80 | 27 |
| $TiO_2$/GO | 97.5 | 140 | 10 |

studied against the notorious *E. coli* (Fig. 10). Fig. 10a shows an image of substantial *E. coli* growth in the absence of any material. The antibacterial activity of pure $TiO_2$ is generally observed to be limited by its inherent large bandgap. As shown in Fig. 10b, a slight antibacterial activity was observed against *E. coli*, where $1.71 \times 10^{12}$ CFU $mL^{-1}$ of microbial culture is evident in the presence of 5 mg $mL^{-1}$ of $TiO_2$. For CuSe samples, substantial bactericidal activity was observed, and only $2.3 \times 10^{11}$ CFU $mL^{-1}$ were present for the same concentration. Increased antibacterial activity was observed for the composite samples. By increasing the CuSe content in the $TiO_2$–CuSe composites, the antibacterial activities were substantially enhanced as the CFU $mL^{-1}$ values of $7.1 \times 10^{11}$ and $1 \times 10^{10}$ are recorded for AK-1 and AK-4 respectively, thus making them ideal materials for combating the *E. coli* related infections. The use of composite materials constructed from two semiconducting materials, such as $TiO_2$ and CuSe, offer added protection against multidrug-resistant bacteria and biofilms through the following two very distinct pathways.

The superior antibacterial activity of $TiO_2$–CuSe composites could be attributed to the ability of the composite to release $Cu^{2+}$ ions, which can interact with the sulfur and phosphorus-

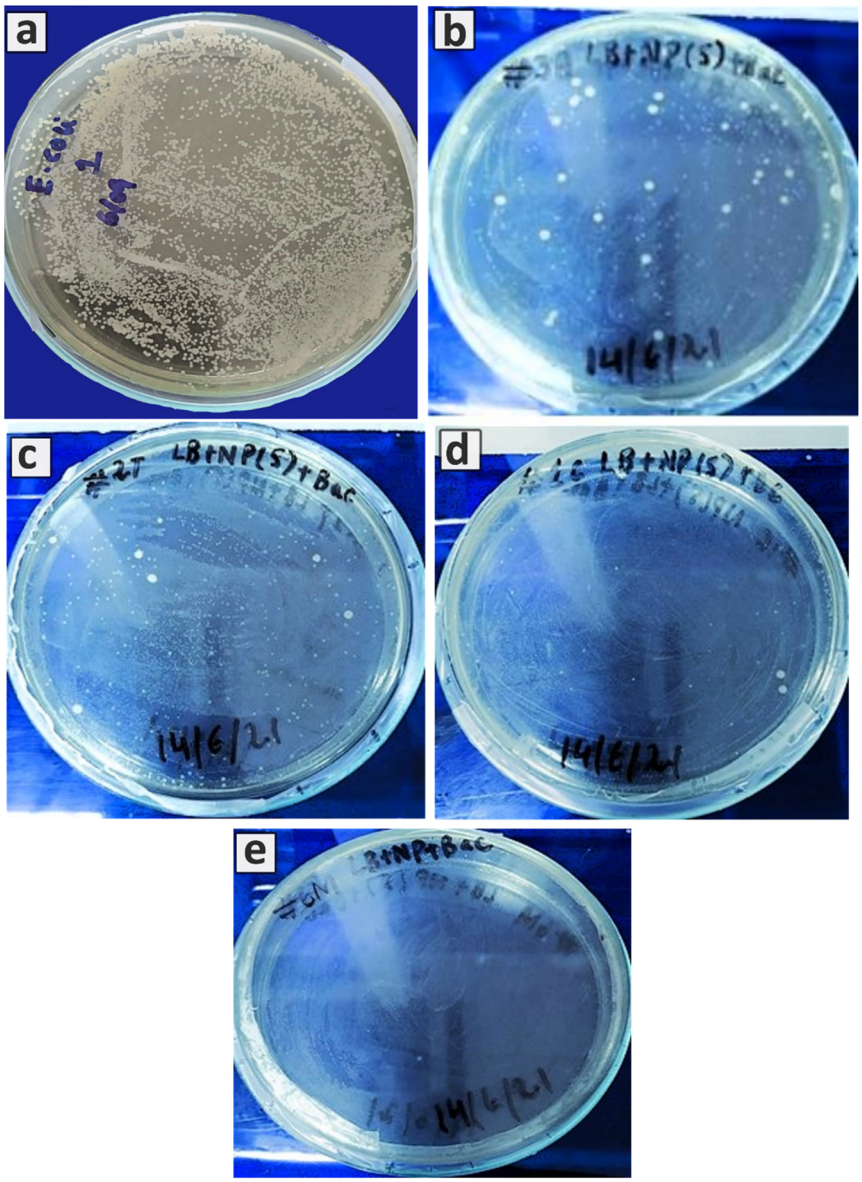


Fig. 10 Antibacterial activity of (a) control (b) $TiO_2$ (c) CuSe (d) AK-1 (e) AK-4.

containing proteins and DNA molecules.[29] The affinity of Cu for S can result in the breakage of the thiol bridge, which can disrupt the tertiary protein structure, hence killing the bacteria. In addition, $Cu^{2+}$ ions can enter through the cell membrane and chelate with the DNA of the bacteria to disturb its cellular biochemical pathways.[30] Furthermore, the released Cu and Ti ions can induce changes in the 3D structure of the enzymes, leading to a change in the active sites of enzymes. The exposure of the composite materials to visible light can excite its electrons from the valence band to the conduction band, resulting in the formation of charge carriers i–e electron/hole ($e^-/h^+$) pairs. Interaction of $e^-/h^+$ with the surrounding oxygen molecules such as water and hydroxyl ions can produce $^{\bullet}OH$ radicals, which have the ability to effectively kill the bacterial cell by penetrating the cell membrane, denaturing the cell proteins, fragmenting the DNA, and inactivating the enzymes.[31,32]

## 4. Conclusions

$TiO_2$–CuSe composites with varying content of CuSe were synthesized and their physicochemical features were investigated for applications in antibacterial and wastewater remediation. The crystalline structure of $TiO_2$, CuSe and their composites was confirmed by XRD and Raman spectroscopy. The surface morphology of the prepared samples revealed agglomerated features of NPs. Furthermore, the light-harvesting capability of $TiO_2$–CuSe composites was substantially enhanced compared to their individual components. For a higher amount of CuSe in the $TiO_2$–CuSe composites, there was a red-shift in absorption edge, and the bandgap value was determined to be 2.91 eV. The prepared photocatalysts were exploited for their efficiency against MB dye removal under visible light illumination. Among them, $TiO_2$–CuSe composite with 20% CuSe content revealed impressive efficiency against MB dye and degraded 98% MB in 60 min. The removal efficiency followed the order: AK-4 > AK-3 > AK-2 > AK-1. Furthermore, the $TiO_2$–CuSe composites showed considerably superior antibacterial activity against *E. coli*, which is attributed to the efficient linking of Cu with the biomolecules to disrupt the tertiary structure of the protein and biological processes of the bacteria. The findings of this work are novel and may be utilized for future applications in wastewater treatment and waterborne diseases.

## Data availability

All data generated or analyzed during this study are included in this article.

## Conflicts of interest

The authors declare no conflicts of interest.

## Acknowledgements

The authors would like to thank the generous support from the Researchers Supporting project number (RSPD2024R981), King Saud University, Riyadh, Saudi Arabia. Prof. Dr Sonia Zulfiqar is highly thankful for the support provided by the Statutory City of Ostrava, Czechia, through the Research Grant "Global Experts". Prof. Cochran and Zulfiqar are thankful to the National Science Foundation for financial support through research grants NSF-2113695, NSF-2132200 and NSF-2242763.

## References

1 M. Hassanpour, H. Safardoust-Hojaghan and M. Salavati-Niasari, *J. Mol. Liq.*, 2017, **229**, 293–299.
2 S. S. Hashmi, M. Shah, W. Muhammad, A. Ahmad, M. A. Ullah, M. Nadeem and B. H. Abbasi, *J. Indian Chem. Soc.*, 2021, **98**(4), 100019.
3 C. Wang, Y. Zhou, Y. Sun, G. Guo, Q. Fu, Z. Xiong and Y. Liu, *Diam. Relat. Mater.*, 2018, **89**, 197–205.
4 S. Zaman, *J. Environ. Prot.*, 2014, **5**, 42.
5 G. Crini and E. Lichtfouse, *Environ. Chem. Lett.*, 2019, **17**, 145–155.
6 D. R. Jones, V. Gomez, J. C. Bear, B. Rome, F. Mazzali, J. D. Mcgettrick, A. R. Lewis, S. Margadonna, W. A. Al-Masry and C. W. Dunnill, *Sci. Rep.*, 2017, **7**, 1–16.
7 R. Maas and S. Chaudhari, *Process Biochem.*, 2005, **40**, 699–705.
8 M. S. S. Danish, L. L. Estrella, I. M. A. Alemaida, A. Lisin, N. Moiseev, M. Ahmadi, M. Nazari, M. Wali, H. Zaheb and T. Senjyu, *Metals*, 2021, **11**, 80.
9 X. Zhu, L. Pei, R. Zhu, Y. Jiao, R. Tang and W. Feng, *Sci. Rep.*, 2018, **8**, 1–14.
10 R. Wang, K. Shi, D. Huang, J. Zhang and S. An, *Sci. Rep.*, 2019, **9**, 1–9.
11 C. Hou, B. Hu and J. Zhu, *Catalysts*, 2018, **8**, 575.
12 L. Ye and Y. Liang, *Phys. B*, 2024, **674**, 415579.
13 D. Chen, Y. Cheng, N. Zhou, P. Chen, Y. Wang, K. Li, S. Huo, P. Cheng, P. Peng, R. Zhang, L. Wang, H. Liu, Y. Liu and R. Ruan, *J. Clean. Prod.*, 2020, **268**, 121725.
14 Z. Zhang, Y. Ma, X. Bu, Q. Wu, Z. Hang, Z. Dong and X. Wu, *Sci. Rep.*, 2018, **8**, 1–11.
15 F. Haque, T. Daeneke, K. Kalantar-Zadeh and J. Z. Ou, *Nano-Micro Lett.*, 2017, **10**, 23.
16 M. Petrović, M. Gilić, J. Ćirković, M. Romčević, N. Romčević, J. Trajić and I. Yahia, *Sci. Sinter.*, 2017, **49**, 167–174.
17 A. Sobhani and M. Salavati-Niasari, *Ceram. Int.*, 2014, **40**, 8173–8182.
18 Y. Mao, H. Zou, Q. Wang and C. Huang, *Sci. China: Chem.*, 2016, **59**, 903–909.
19 K. Patel, G. K. Solanki, K. D. Patel and V. M. Pathak, *J. Phys. Chem. C*, 2021, **125**, 3517–3526.
20 M. Nouri, R. Yousefi, N. Zare-Dehnavi and F. Jamali-Sheini, *Colloids Surf., A*, 2020, **586**, 124196.
21 J. Y. C. Liew, Z. A. Talib, Z. Zainal, M. A. Kamarudin, N. H. Osman and H. K. Lee, *Semicond. Sci. Technol.*, 2019, **34**, 125017.
22 Z. Ali, A. u. Shah, Z. Ali and A. Mahmood, *Mater. Chem. Phys.*, 2020, **249**, 123169.

23 F. Ahmad, R. Hussain, S. U. Khan, A. Shah, M. F. Alajmi, M. Arif, A. Hussain, I. Parveen and S. u. Rahman, *Res. Chem. Intermed.*, 2024, **50**, 2501–2518.
24 N. Wetchakun, S. Chainet, S. Phanichphant and K. Wetchakun, *Ceram. Int.*, 2015, **41**, 5999–6004.
25 Y. Yang, L. Xu, H. Wang, W. Wang and L. Zhang, *Mater. Des.*, 2016, **108**, 632–639.
26 R. Li, Y. Jia, N. Bu, J. Wu and Q. Zhen, *J. Alloys Compd.*, 2015, **643**, 88–93.
27 S. Bibi, A. Ahmad, M. A. R. Anjum, A. Haleem, M. Siddiq, S. S. Shah and A. A. Kahtani, *J. Environ. Chem. Eng.*, 2021, **9**, 105580.
28 L. Zhou, Y. Deng, Y. Ren, H. L. Poon, W. Y. Chu, H. Wang and Y. K. Chan, *J. Chem. Eng.*, 2024, **482**, 148978.
29 N. Mbewana-Ntshanka, M. Moloto and P. Mubiayi, *J. Nanomater.*, 2021, 675145.
30 Y. Li, J. Yu, W. Zhang, J. Shan, H. Chen, Y. Ma and X. Wang, *J. Colloid Interface Sci.*, 2024, **666**, 434–446.
31 A. Villegas-Fuentes, A. Rosillo-De La Torre, A. R. Vilchis-Nestor and P. A. Luque, *Chemosphere*, 2023, **339**, 139577.
32 S. U. Khan, G. O. Eren, N. Atac, A. Onal, M. H. Qureshi, F. K. Cooper, T. Almammadov, S. Kolemen, M. Sahin, F. Can and S. Nizamoglu, *J. Chem. Eng.*, 2024, **480**, 148140.